nature chemistry

ARTICLES

https://doi.org/10.1038/s41557-020-00562-5

Check for updates

Partitioning the interlayer space of covalent organic frameworks by embedding pseudorotaxanes in their backbones

Xing Li[1], Hai-Sen Xu[1], Kai Leng[1], See Wee Chee[2,3], Xiaoxu Zhao[1], Noopur Jain[2,3], Hai Xu[1], Jingsi Qiao[4], Qiang Gao[1], In-Hyeok Park[1], Su Ying Quek[2,4], Utkur Mirsaidov[2,3] and Kian Ping Loh[1]✉

Mono- or few-layer sheets of covalent organic frameworks (COFs) represent an attractive platform of two-dimensional materials that hold promise for tailor-made functionality and pores, through judicious design of the COF building blocks. But although a wide variety of layered COFs have been synthesized, cleaving their interlayer stacking to obtain COF sheets of uniform thickness has remained challenging. Here, we have partitioned the interlayer space in COFs by incorporating pseudorotaxane units into their backbones. Macrocyclic hosts based on crown ethers were embedded into either a ditopic or a tetratopic acylhydrazide building block. Reaction with a tritopic aldehyde linker led to the formation of acylhydrazone-based layered COFs in which one basal plane is composed of either one layer, in the case of the ditopic macrocyclic component, or two adjacent layers covalently held together by its tetratopic counterpart. When a viologen threading unit is introduced, the formation of a host–guest complex facilitates the self-exfoliation of the COFs into crystalline monolayers or bilayers, respectively.

Covalent organic frameworks are a class of porous crystalline materials constructed via covalent integration of molecular organic building units[1–6]. Depending on the space where the covalent linkages propagate, COFs have been classified into 1D, 2D and 3D materials[7–10]. Strictly speaking, 2D COFs are quasi-2D in nature due to the non-covalent interaction present between layers. The generation of graphene-like sheets from 2D COFs by mechanical[11–14] or chemical exfoliation[15] has the potential to create a whole new class of molecularly thin organic 2D materials. However, the relatively weak covalent linkages (boronate ester, imine and so on) as well as the strong interlayer binding forces result in ill-defined cleavage planes, and render it highly challenging to exfoliate 2D COFs to produce large-size, few-layer ($n < 5$) sheets. An alternative method to control the thickness of COFs involves interface-confined growth[16–18], but this is difficult to scale up. So far, growth of COF monolayers is still highly challenging[19], and the most successful example in terms of highly crystalline growth has been demonstrated using surface-assisted methods[20–23]. The search is on for ways to program weak interlayer linkages into COFs to allow easy exfoliation into monolayer sheets, hopefully with well-defined thickness. Decoupling the interlayer stacking to make turbostratic COFs (in which the planes are randomly offset with respect to one another) should weaken the interlayer binding force and facilitate exfoliation. A totally different approach that has not been considered thus far involves the integration of mechanically interlocked molecular architectures (MIMAs)[24–27] into quasi-2D COFs. Depending on the number of COF layers that can be interlocked per molecular complex, this may afford a strategy to partition the interlayer space into pseudo-unit cells. We have been inspired by the installation of rotaxane or catenane units into metal–organic frameworks (MOFs)[28,29]. We envisaged that the structure of MIMAs can be exploited to mechanically bond or complex with a specific number of COF layers, thus generating pseudo-periodicity when the MIMAs are spaced out regularly along the *c*-axis. As shown in Fig. 1a, the number of COF layers complexed can be controlled by modifying the building units. Catenanes can be used to link the macrocyclic building blocks to interlock a specific number of COF layers. Ditopic macrocyclic building blocks modified with rotaxanes or catenanes can be utilized to construct COFs with odd numbers of layers.

Here, we have incorporated pseudorotaxane units into the COF scaffold (Fig. 1) as a proof of concept. These pseudorotaxane host–guest units are composed of a viologen threading unit and a crown ether macrocycle. The macrocyclic building block is composed of a crown ether bearing either ditopic or tetratopic hydrazides. Using these crown-ether building units, we construct [2+3] and [4+3] 2D COFs respectively sandwiched by macrocycles between the layers. The solids are held together by strong non-covalent interactions and crystallize as quasi-2D COFs. The unique features of our design include: (1) in the COF constructed from the ditopic crown-ether hydrazide, a unit cell forms with two-layer thickness but only one layer of hydrazone linkages, while the hydrazone-unsubstituted phenyl rings of the macrocycles are in another layer; (2) in the COF constructed from the tetratopic crown-ether hydrazide, two layers of COF planes are linked covalently by the macrocycles, forming a pseudo-unit cell containing a bilayer. To the best of our knowledge, such a 2D COF design incorporating building blocks that bear out-of-plane covalent bonds embedded within a bilayer unit cell has not been explored previously. In addition, the macrocycles also serve as hosts for viologens, thereby forming pseudorotaxane units in the COF. From a supramolecular perspective, we are generating pseudorotaxane complexes in situ within bilayer COF sheets, which weakens the interlayer stacking forces and allows self-exfoliation of the material via electrostatic repulsion.

[1]Department of Chemistry, National University of Singapore, Singapore, Singapore. [2]Department of Physics, National University of Singapore, Singapore, Singapore. [3]Centre for BioImaging Sciences, Department of Biological Sciences, National University of Singapore, Singapore, Singapore. [4]Centre for Advanced 2D Materials and Graphene Research Centre, National University of Singapore, Singapore, Singapore. ✉e-mail: chmlohkp@nus.edu.sg

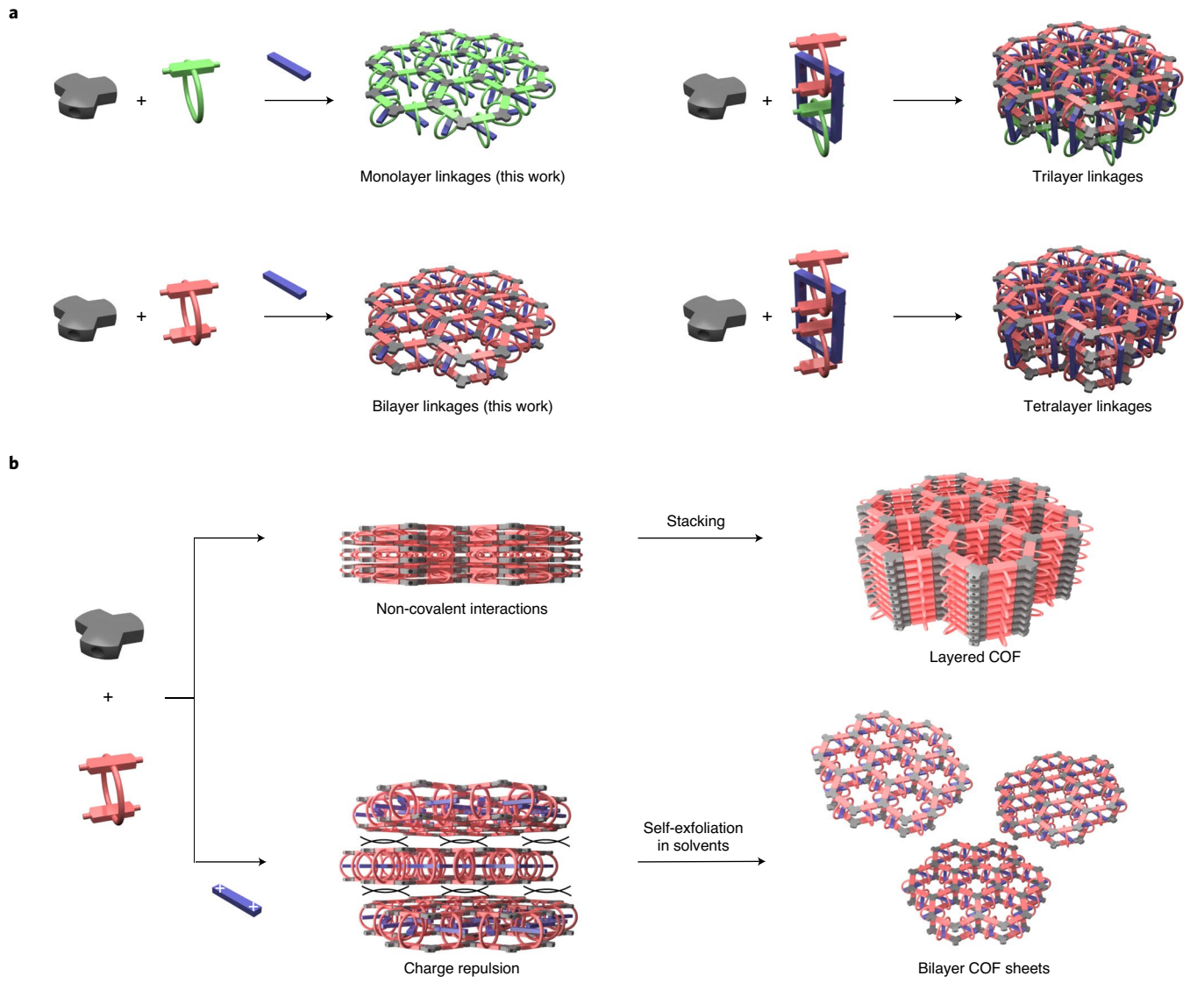

Fig. 1 | A general strategy for design and construction of self-exfoliated COFs with well-defined layer numbers of covalent linkages. a, Construction of 2D COFs with targeted layer numbers via mechanical bonds. **b**, Construction of self-exfoliated COF bilayers via insertion of ionic threads. **c**, Chemical structures of the schematic building units. The conventional COF growth method affords quasi-2D materials driven by the strong non-covalent interactions between layers. When a macrocycle host is anchored onto the building block, it provides a site for binding ionic species. During the growth process, these ionic threads can create electrostatic repulsive forces between layers and hence disrupt the stacking order, giving rise to self-exfoliated COF bilayers.

Results and discussion

Design and synthesis of macrocycle-based COFs. Recently, we have reported that acylhydrazone 2D COFs prefer to be stacked anti-parallel due to strong interlayer dipole interactions[30], which renders it challenging for the exfoliation of ultrathin sheets. Our motivation for installing bulky pseudorotaxanes in the COF building units is to inhibit interlayer interactions via steric hindrance and electrostatic repulsion and to create more disordering along the *c*-axis, thus

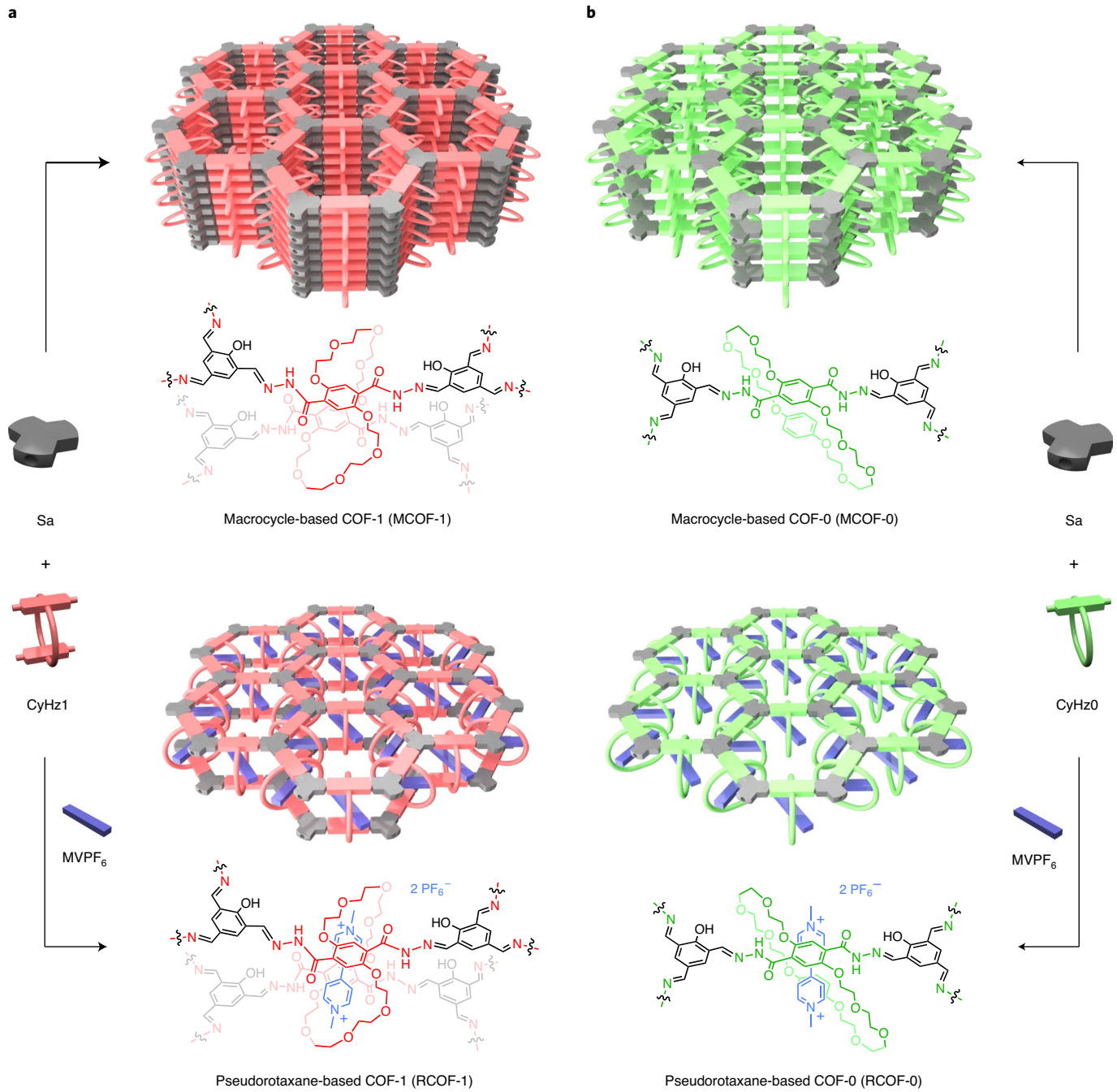

Fig. 2 | Synthesis of macrocycle- and pseudorotaxane-based COFs. a, MCOF-1 was synthesized using a tritopic aldehyde node and a tetratopic crown-ether macrocycle with two hydrazide moieties (**CyHz1**) holding together two adjacent COF layers. The COF layers are stacked in an antiparallel stacking fashion, with strong interlayer dipole interactions. Self-exfoliated RCOF-1 was synthesized using the same building units as MCOF-1 but in the presence of methyl viologen as the interfering agent for stacking disruption. **b**, MCOF-0 and RCOF-0 were synthesized using the same tritopic aldehyde node but with a ditopic crown-ether linker (**CyHz0**). Diametrically opposed to its hydrazide functionality, **CyHz0** features a hydrazide-unsubstituted phenyl ring; this is to prevent strong dipole interaction between adjacent COF layers.

facilitating the exfoliation of 2D COFs. As shown in Fig. 2, the repeating structure is based on a sandwich-like building block that interlocks two COF layers with one macrocycle. The tetratopic linker, namely **CyHz1**, bears a bis-*p*-phenylene 34-crown-10 macrocycle with four hydrazide groups for connection. The crown ether macrocycle binds specifically to ionic species such as sodium ions and viologens[31]. The *para*-phenylene units can undergo π–π interactions, and hydrogen bonding between the N–H and O moieties planarizes the building blocks, ensuring that the network can be formed in a 2D fashion even in the presence of the bulky complexes. Without the complexation of viologen species, the dipole interaction between the acylhydrazone linkages and ether side chains gives rise to ordered close stacking of 2D COFs in antiparallel conformation. To verify these assumptions, we synthesized a macrocycle-based COF without a threading ionic species (that is, MCOF-1) via the condensation of 2,4,6-triformylphenol (**Sa**) and **CyHz1** in a solution of 10:1 (v/v) mesitylene and 6 M aqueous acetic acid at 120 °C over seven days. The good crystallinity of MCOF-1 was confirmed by

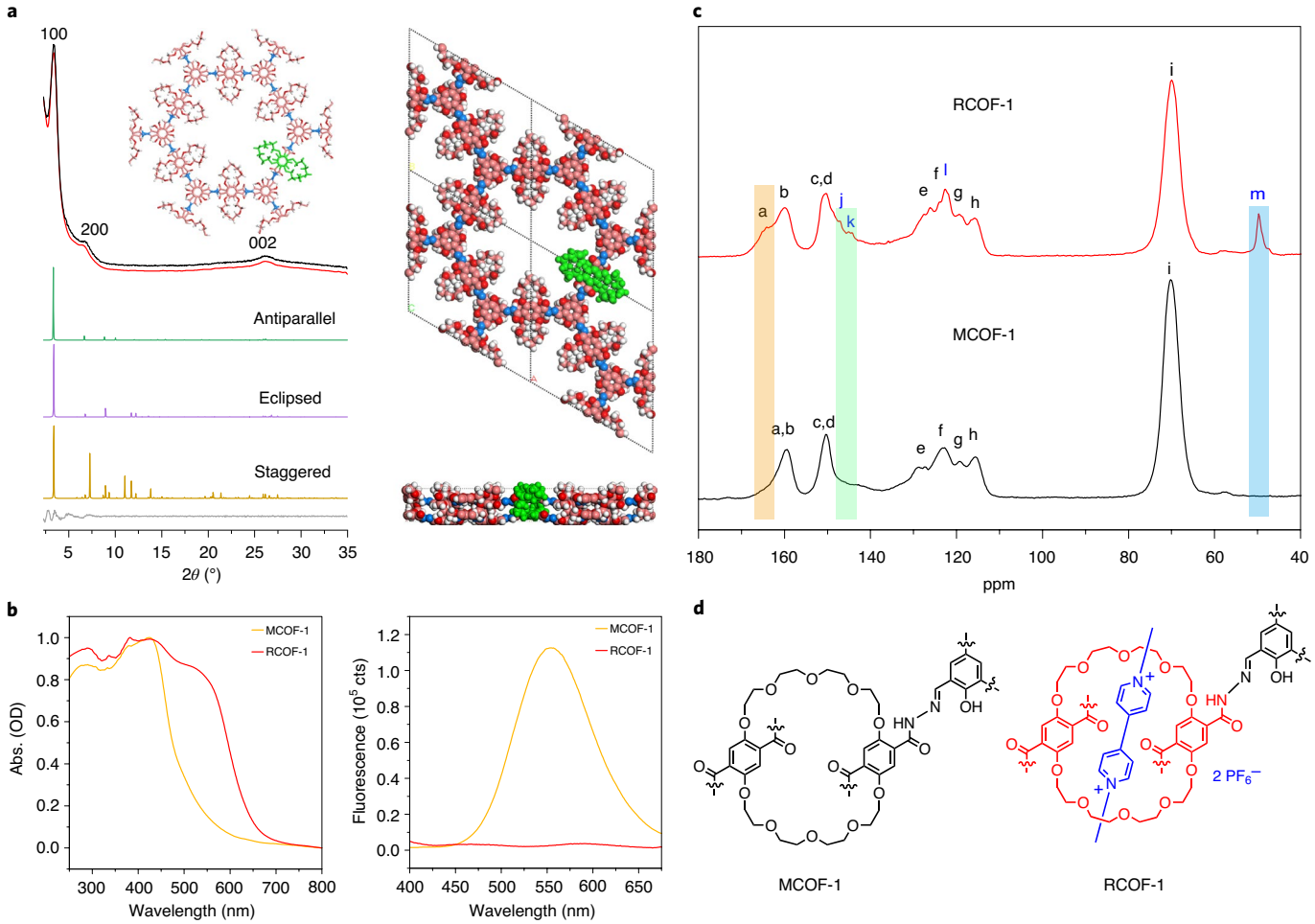

Fig. 3 | Characterization of the crystallinity of MCOF-1 and the pseudorotaxane complexation in RCOF-1. a, Characterization by powder X-ray diffraction (PXRD). Left, PXRD patterns of MCOF-1: experimental (black), Pawley-refined (red), their difference (grey), simulated antiparallel stacking (green), eclipsed stacking (purple), and staggered stacking (yellow). Right, PXRD-refined crystal structures of the antiparallel stacking MCOF-1 viewed along (top) and perpendicular to (bottom) the *c*-axis. Atom colour code: C, pink; N, blue; O, red; H, white; a single macrocycle, green. **b**, Characterization of MCOF-1 and RCOF-1 in the bulk form. Solid-state UV-vis spectra (left) and solid-state fluorescence spectra (right). Abs, absorbance; cts, counts. **c**, Solid-state CP/MAS ^{13}C NMR spectra of MCOF-1 and RCOF-1. **d**, Structures of MCOF-1 and RCOF-1, with the viologen threading unit shown in blue.

powder X-ray diffraction (PXRD), indicating that the incorporation of macrocycles (hosts) in the absence of threading units (guests) did not disrupt the in-plane or out-of-plane crystallization (Fig. 3). The PXRD pattern of MCOF-1 exhibits two intense peaks at 3.36 and 6.82°, which correspond to the (100) and (200) facets, respectively. The peak at 26.2° corresponds to the (002) facet of MCOF-1. The Pawley-refined PXRD pattern (Material Studio 2016) agrees with the experimental results well, with R_p and R_{wp} values of 1.84 and 2.26%, respectively. To determine the crystal structure of MCOF-1, the bilayer structure was simulated for antiparallel, eclipsed and staggered stacking conformations (Fig. 3a and Supplementary Fig. 11). The simulated PXRD pattern of the antiparallel form shows a better agreement with the experimental result than the other forms, suggesting that antiparallel stacking is the preferred structure. Based on the above results, we concluded that MCOF-1 adopts antiparallel stacking and has a *P*6 space group unit cell, with Pawley-refined cell parameters $a=b=30.5769$ Å, $c=7.0416$ Å, $\alpha=\beta=90°$, and $\gamma=120°$. Furthermore, we measured synchrotron PXRD of MCOF-1, which reveals diffraction rings corresponding to various facets in the crystal (Supplementary Fig. 7). The flexible polyether side chains are most likely disordered and crosslinking between COF layers could occur in MCOF-1.

To further disrupt the interlayer interaction, we designed a ditopic crown-ether hydrazide (**CyHz0**) and synthesized MCOF-0 under similar conditions to MCOF-1 (Fig. 2). The role of a layer of hydrazone-unsubstituted phenyl rings in MCOF-0 is to disrupt the dipole interaction in such acylhydrazone COFs. The PXRD pattern of MCOF-0 exhibits two peaks at 3.43 and 6.88°, corresponding to the (100) and (200) facets, respectively (Supplementary Fig. 8). Compared to MCOF-1, there is a much-broadened peak at 24.87°, indicating an increased π–π stacking distance of MCOF-0. This is due to the unusual corrugated structure of MCOF-0, which lacks one layer of **Sa** linkers and hydrazone linkages in the unit cell compared with MCOF-1, leading to disrupted stacking of the COF layers. Through such a design, the dipole interaction in MCOF-0 is expected to be weakened, further facilitating the exfoliation process upon complexation of ionic species. The broadened PXRD peaks in MCOFs are probably due to the high conformational flexibility of the double-decker structures with mixed stacking orders such as slip-eclipsed and antiparallel stacking, which could not be fully resolved at the current stage. The (100) planes of MCOFs were further confirmed by selected area electron diffraction (SAED), in which the corresponding *d*-spacings of 2.4 nm are consistent with the crystal lattice (Supplementary Figs. 25 and 27).

Embedding pseudorotaxane moieties into COFs. The as-synthesized MCOF-0 and MCOF-1 are difficult to exfoliate in solution due to their strong interlayer interactions (Supplementary Figs. 22 and 24). We examined how the COF crystallization process is affected if threading units are added during COF synthesis. By inserting ionic threads into the macrocycles of MCOF-1 and MCOF-0, pseudorotaxane-based COFs (RCOF-1 and RCOF-0) can be generated; the interlayer COF stacking is weakened due to the presence of ionic repulsion, which predisposes the COF to be self-exfoliated. For this purpose, we have chosen a classic pseudorotaxane complex of bis-*p*-phenylene 34-crown-10 and methyl viologen. Using synthetic conditions similar to those employed for MCOF-1, pseudorotaxane-based COF-1 (RCOF-1) was synthesized in the presence of a stoichiometric amount of methyl viologen hexafluorophosphate (**MVPF$_6$**). Since the RCOF-1 flakes are ultrathin, synchrotron-based grazing incidence XRD (GIXRD) was employed to observe the (100) peak; the details are provided in later sections. The (100) peak of RCOF-1 is weak using conventional Cu source PXRD (Supplementary Figs. 13 and 14), which may be due to random restacking of the exfoliated flakes. However, there is an increase of interlayer distance in bulk RCOF-1 compared with MCOF-1 as observed by conventional PXRD, suggesting the presence of interfering agents between COF bilayers in RCOF-1.

The formation of pseudorotaxane complex RCOF-1 is expected to cause the redistribution of electrons, leading to energy shifts of bonding states. Solid-state UV-vis absorption spectroscopy, solid-state fluorescence spectroscopy, Fourier transform infrared (FT-IR) spectroscopy, and NMR spectroscopy were used to monitor these interactions. Solid-state UV-vis absorption spectra reveal a decrease in the optical bandgap from 2.12 eV for MCOF-1 to 1.83 eV for RCOF-1 (Fig. 3b, left). The redshifted band at 550 nm is characteristic of the charge-transfer process upon crown ether–viologen complexation[31], suggesting the successful insertion of **MVPF$_6$** into the COF macrocycles. In addition, MCOF-1 becomes fluorescent (λ_{max} = 550 nm) because of restricted intramolecular bond rotation (RIR) due to hydrogen bonding[32] (Fig. 3b, right). By contrast, the quenched fluorescence in bulk RCOF-1 suggests the presence of charge transfer in the COF pseudorotaxane moieties, which results in the quenching of the photo-excited energy. Solid-state cross-polarization/magic-angle-spinning (CP/MAS) ^{13}C NMR experiments further confirm successful complexation between the crown-ether macrocycle and viologen in RCOF-1 (Fig. 3c), as judged from the appearance of a new peak at 49.7 ppm corresponding to the methyl carbon atom (**m**) connected to the pyridinium salt, suggesting the presence of methyl viologen in RCOF-1. Moreover, the amide carbon (**a**) and phenyl carbon (**b**) atoms exhibit similar chemical shifts (159.6 ppm) in MCOF-1. By contrast, the peak corresponding to the amide carbon (**a**) atom shifts to 164.3 ppm in RCOF-1, indicating a loss of electron density. This is consistent with redistribution of the π-electron density upon pseudorotaxane complexation[33]. To further study the pseudorotaxane complexation in RCOF-1, we synthesized a single crystal of the molecular analogue representing the macrocycle–viologen complex (Supplementary Fig. 6). A similar trend in the FT-IR spectra can be seen in both RCOF-1 and the molecular analogue due to complexation with viologen: the ring-stretching bands (8a and 19a) of the viologen (**MVPF$_6$**) redshift and the C=O stretching band of the carbonyl group on the macrocycle blueshifts, suggesting the presence of pseudorotaxane complexes in RCOF-1. This result agrees well with the solid-state ^{13}C NMR data, in which the π-electron density is transferred from electron-rich macrocycle moieties to electron-deficient viologens upon complexation[33,34]. Both solid-state NMR (Fig. 3c) and FT-IR (Supplementary Fig. 6) data reveal that the crown-ether–viologen complexation does not affect the chemical integrity of the basal planes during COF growth. RCOF-0 was also prepared and characterized using similar methods (see Supplementary Information, Supplementary Figs. 3, 9 and 10).

Exfoliation of COF monolayers and bilayers. Unlike MCOF-1, which is insoluble and forms thick aggregates (Fig. 4a), pseudorotaxane RCOF-1 disperses well in a wide range of solvents (Fig. 4 and Supplementary Fig. 22) because of its positively charged pyridinium ions in the viologen units. Global charge neutralization is maintained by the PF_6^- counterions, such that the individual flakes are weakly bound by ionic forces. Slight mechanical agitation disturbs the ionic balance and allows the weakly bonded, charged 2D bilayer flakes to be readily exfoliated. The fluorescence that was quenched in bulk RCOF-1 was turned on in RCOF-1 dispersions, and the Tyndall effect could be observed, as shown in Supplementary Figs. 22 and 23. Transmission electron microscopy (TEM) (Fig. 4b) and atomic force microscopy (AFM) (Fig. 5) reveal the 2D sheet-like morphology of the exfoliated RCOFs. The crystallinity of these flakes was further characterized by synchrotron-based grazing incidence X-ray diffraction (GIXRD), SAED, low-dose high-resolution TEM (HRTEM) and Q-plus AFM. To investigate the crystallinity of exfoliated RCOF-1 flakes, we measured synchrotron-based GIXRD of the exfoliated RCOF-1 on the silica substrate (Fig. 4d, top and bottom). In the direction parallel to the substrate, GIXRD of RCOF-1 flakes exhibits three peaks at 0.258, 1.123, 1.368 Å^{-1}, which correspond to *d*-spacings of 24.4, 5.6 and 4.6 Å and are assigned to (100), (410) and (510) facets, respectively. The appearance of (100) facet along the *xy*-plane suggests the exfoliated RCOF-1 flakes inherit the in-plane crystal structure of MCOF-1. In the direction perpendicular to the substrate, there is only a small peak at 0.438 Å^{-1} (*d*-spacing of 1.4 nm) assignable to (001) facet. The SAED pattern of RCOF-1 flakes agrees well with the X-ray diffraction results, with *d*-spacings of 2.4 and 1.2 nm corresponding to the (100) and (001) planes, respectively (Fig. 4c). To ascertain the thickness of the unit cell we conducted density functional theory (DFT) of RCOF-1 based on the parallel and antiparallel crystal structure (Fig. 5c and Supplementary Figs. 15 and 16). For both stacking modes, the calculated RCOF-1 exhibits a thickness of ~1.1 nm, which is very close to the experimental *d*-spacing for (001) planes derived from GIXRD and SAED. The slight thickness increase in the real RCOF-1 flakes is probably caused by the unit-cell expansion in the *z*-direction after exfoliation due to the flexible structure. The low-dose HRTEM lattice fringes show a *d*-spacing of 5.9 Å which is consistent with the *d*-spacing of 5.6 Å observed in in-plane GIXRD, which corresponds to the (410) facet of RCOF-1 (Fig. 4e, f). Furthermore, we conducted Q-plus AFM measurement of the exfoliated RCOF-1 on Au(111) substrate. The Q-plus AFM scan exhibits nice lattice fringes with a *d*-spacing of 4.7 Å, which is consistent with the (510) peak (*d*-spacing = 4.6 Å) in the in-plane GIXRD (Fig. 4g, h). The evidence suggests that exfoliated RCOF-1 flakes maintain their crystalline integrity.

AFM studies reveal that >80% of the exfoliated flakes are 2 nm thick for RCOF-0 and 4 nm thick for RCOF-1 (Fig. 5). The different thickness distribution for these exfoliated flakes validated our concept that tailoring the structure of the macrocycle interlocking with the COF provides a handle to control the thickness of the exfoliated flakes. The incorporation of pseudorotaxane complexes in MCOFs also ensures the easy exfoliation of these COFs into few layers via ionic repulsion. Moreover, the non-symmetrical corrugated structure induced by the ditopic crown-ether building unit further weakens the stacking between RCOF-0 layers, allowing the exfoliation of much thinner flakes than RCOF-1. Owing to the effects of tip–surface interaction, surface roughness and trapped solvent, the AFM-measured thickness is typically larger than the theoretical value of the unit cell constant by several times[35]. Therefore, the AFM thickness of a single unit cell is measured to be 2 nm even though the DFT-simulated thickness is 1.1 nm (Fig. 5c and Supplementary

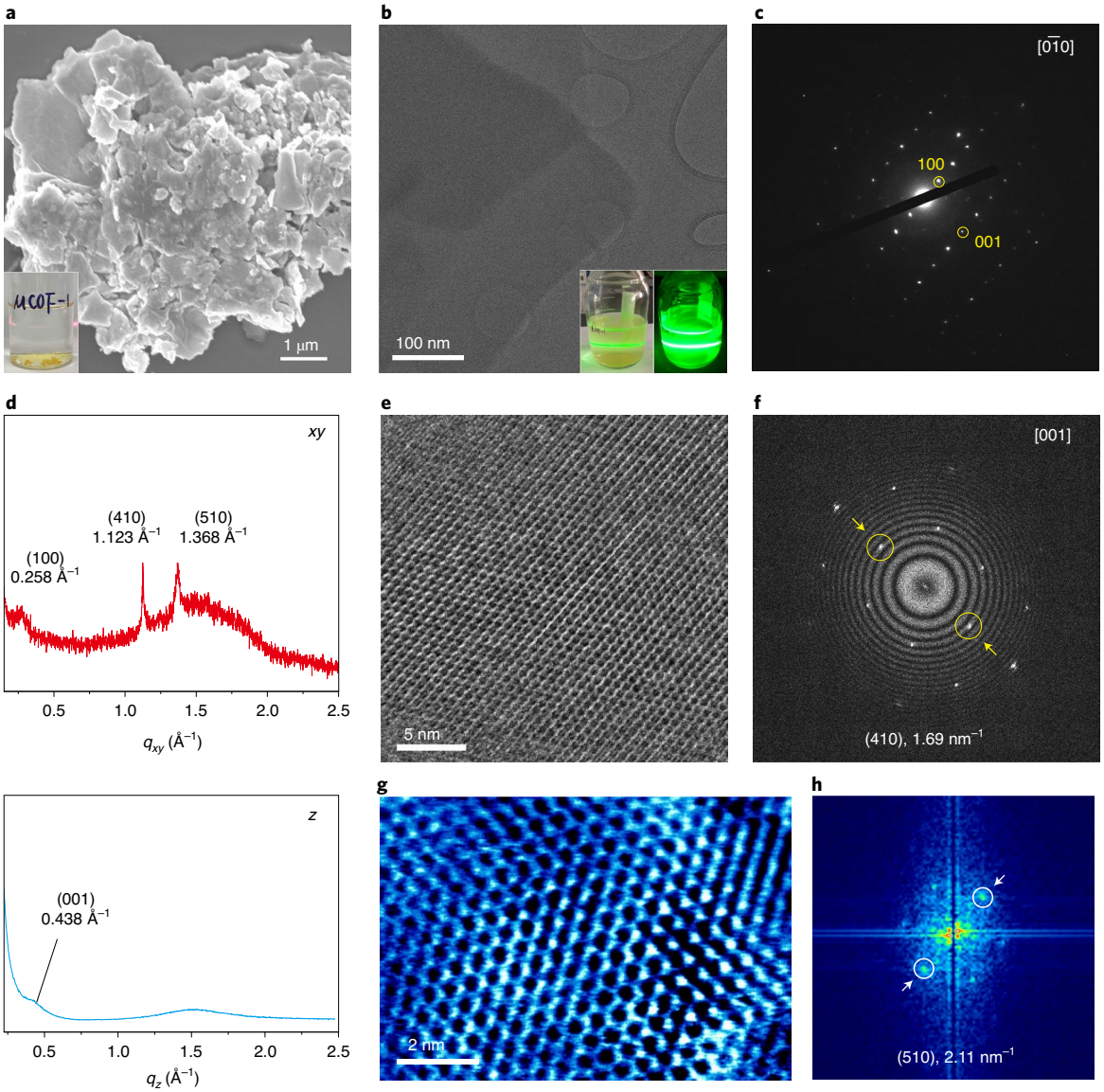

Fig. 4 | Exfoliation of RCOF-1 and characterization of its crystallinity. a, SEM image of MCOF-1 after sonication in ethanol for 30 min. **b**, TEM image of RCOF-1 flake after sonication in ethanol for 5 s (inset: mass RCOF-1 dispersion exhibiting the Tyndall effect). **c**, SAED pattern of RCOF-1 taken at cryogenic temperature, *d*-spacings of 2.4 nm and 1.2 nm corresponding to (100) and (001) planes, respectively (zone-axis is along [0—10] direction). **d**, GIXRD patterns of exfoliated RCOF-1 on silica substrate at parallel (top, red) and perpendicular (bottom, blue) directions to the substrate. **e**, Low-dose HRTEM image of exfoliated RCOF-1 with lattice fringes assigned to the (410) facet (zone-axis is along [001] direction). **f**, Fast Fourier transform (FFT) of lattice fringes from **e**. **g**, Q-plus AFM image of exfoliated RCOF-1 on gold substrate with lattice fringes assigned to the (510) facet. **h**, The FFT of lattice fringes from **g**.

Figs. 15–17). Indeed, in a zoom-in area, we observed RCOF-1 flakes as thin as ~2 nm, with a consistent step height increase of ~2 nm (Fig. 5d), thus we infer that this value corresponds the to unit-cell thickness, and that a thickness of 4 nm, which is the predominant flake thickness observed, corresponds to the thickness of two unit cells (Fig. 5e, f). According to the single-crystal structures of the model compounds (Supplementary Figs. 6a and 10), the two atomic layers crosslinked via the crown ethers should be antiparallel-stacked in RCOF-1, while the crown-ether-bonded phenyl rings should be parallel-stacked onto the layers with acylhydrazone linkages in RCOF-0. The presence of dipole–dipole interactions in these frameworks originates from permanent bond dipole moments in the acylhydrazone linkages and side chains, and this causes the antiparallel-stacked structure to be preferred[30]. This also implies that there is a tendency for the layers to bind via electrostatic interactions, which may explain why AFM studies revealed that the exfoliated RCOF-1 flakes had predominantly double unit-cell thickness (see illustration in Supplementary Fig. 33). By contrast, RCOF-0 has a different design: the crown ether building units place a layer of phenyl rings without acylhydrazone linkages, thus separating the two layers with acylhydrazone linkages and weakening the dipole–dipole interactions; as a result, there is a greater chance to exfoliate an RCOF-0 flake of a single unit-cell thickness.

Conclusion

We have developed a strategy to disrupt the stacking order in 2D COFs by integrating pseudorotaxane moieties into their backbone functionalities. Compared to surface-confined growth, our method is highly useful for the scalable production of monolayer COFs with controllable thickness. The interlayer space in COFs can be

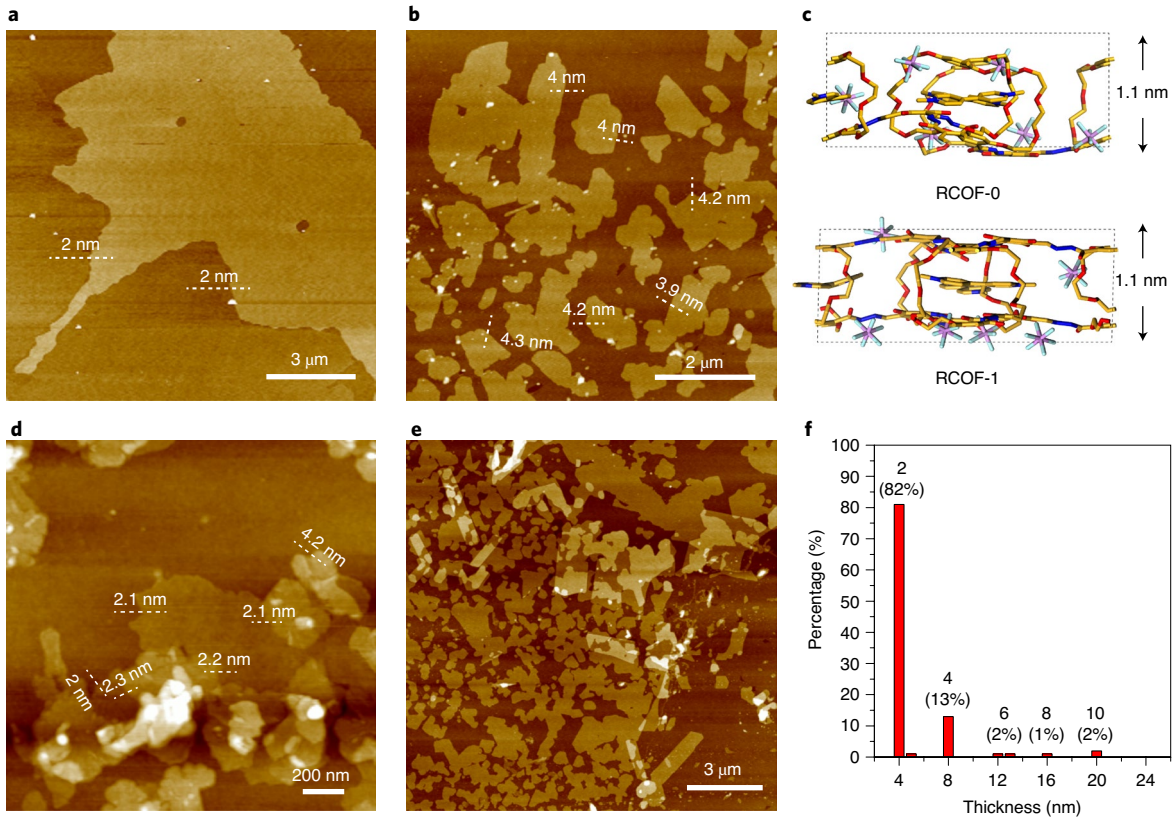

Fig. 5 | AFM study of RCOF-0 and RCOF-1. a, AFM image of a big RCOF-0 flake with thickness of 2 nm. **b**, AFM image of RCOF-1 flakes with thickness of 4 nm. **c**, Theoretical thickness of the DFT-optimized unit cells of RCOF-0 and RCOF-1. Atom colour code: C, orange; O, red; N, navy blue; P, purple; F, light blue; H atoms are omitted. **d**, Zoomed-in AFM image of RCOF-1 showing step increase of 2 nm. **e**, A 15 × 15 μm^2 AFM image of exfoliated RCOF-1 flakes on silica substrate. **f**, Thickness distribution histogram of RCOF-1 flakes in **e**, as measured by AFM, where the thickness equivalent of unit cells is indicated.

partitioned into separable, pseudo-unit cells of *n*th layer thickness by interlocking an *n*th layer COF with molecular knots of appropriate length. The implication is that this method allows 2D organic sheets of well-defined thickness to be exfoliated easily in liquid. From a crystal engineering perspective, pseudorotaxane 2D COFs bridge the field between molecular machines and 2D materials, and we hope that this field will further develop towards the integration of molecular shuttles into COFs that can be responsive to pH, ions, light and electrons.

Online content

Any methods, additional references, Nature Research reporting summaries, source data, extended data, supplementary information, acknowledgements, peer review information; details of author contributions and competing interests; and statements of data and code availability are available at https://doi.org/10.1038/s41557-020-00562-5.

Received: 15 April 2019; Accepted: 11 September 2020;
Published online: 2 November 2020

References

1. Colson,, J. W. & Dichtel,, W. R. Rationally synthesized two-dimensional polymers. *Nat. Chem.* **5**, 453–465 (2013).
2. Ding, S.-Y. & Wang, W. Covalent organic frameworks (COFs): from design to applications. *Chem. Soc. Rev.* **42**, 548–568 (2013).
3. Huang, N., Wang, P. & Jiang, D. Covalent organic frameworks: a materials platform for structural and functional designs. *Nat. Rev. Mater.* **1**, 16068 (2016).
4. Segura, J. L., Mancheno, M. J. & Zamora, F. Covalent organic frameworks based on Schiff-base chemistry: synthesis, properties and potential applications. *Chem. Soc. Rev.* **45**, 5635–5671 (2016).
5. Diercks, C. S. & Yaghi, O. M. The atom, the molecule, and the covalent organic framework. *Science* **355**, eaal1585 (2017).
6. Li,, X., Yadav,, P. & Loh,, K. P. Function-oriented synthesis of two-dimensional (2D) covalent organic frameworks – from 3D solids to 2D sheets. *Chem. Soc. Rev.* **49**, 4835–4866 (2020).
7. Xu, H.-S. et al. Single crystal of a one-dimensional metallo-covalent organic framework. *Nat. Commun.* **11**, 1434 (2020).
8. Côté, A. P. et al. Porous, crystalline, covalent organic frameworks. *Science* **310**, 1166–1170 (2005).
9. El-Kaderi, H. M. et al. Designed synthesis of 3D covalent organic frameworks. *Science* **316**, 268–272 (2007).
10. Lyle, S. J., Waller, P. J. & Yaghi, O. M. Covalent organic frameworks: organic chemistry extended into two and three dimensions. *Trends Chem.* **1**, 172–184 (2019).
11. Berlanga, I. et al. Delamination of layered covalent organic frameworks. *Small* **7**, 1207–1211 (2011).
12. Bunck, D. N. & Dichtel, W. R. Bulk synthesis of exfoliated two-dimensional polymers using hydrazone-linked covalent organic frameworks. *J. Am. Chem. Soc.* **135**, 14952–14955 (2013).
13. Chandra, S. et al. Chemically stable multilayered covalent organic nanosheets from covalent organic frameworks via mechanical delamination. *J. Am. Chem. Soc.* **135**, 17853–17861 (2013).
14. Peng, Y. et al. Ultrathin two-dimensional covalent organic framework nanosheets: preparation and application in highly sensitive and selective DNA detection. *J. Am. Chem. Soc.* **139**, 8698–8704 (2017).
15. Khayum, M. A. et al. Chemically delaminated free-standing ultrathin covalent organic nanosheets. *Angew. Chem. Int. Ed.* **55**, 15604–15608 (2016).
16. Colson, J. W. et al. Oriented 2D covalent organic framework thin films on single-layer graphene. *Science* **332**, 228–231 (2011).
17. Matsumoto, M. et al. Lewis-acid-catalyzed interfacial polymerization of covalent organic framework films. *Chem* **4**, 308–317 (2018).

18. Hao, Q. et al. Confined synthesis of two-dimensional covalent organic framework thin films within superspreading water layer. *J. Am. Chem. Soc.* **140**, 12152–12158 (2018).
19. Zhou, T.-Y., Lin, F., Li, Z.-T. & Zhao, X. Single-step solution-phase synthesis of free-standing two-dimensional polymers and their evolution into hollow spheres. *Macromolecules* **46**, 7745–7752 (2013).
20. Dienstmaier, J. F. et al. Synthesis of well-ordered COF monolayers: surface growth of nanocrystalline precursors versus direct on-surface polycondensation. *ACS Nano* **5**, 9737–9745 (2011).
21. Xu, L. et al. Surface-confined single-layer covalent organic framework on single-layer graphene grown on copper foil. *Angew. Chem. Int. Ed.* **53**, 9564–9568 (2014).
22. Chen, C. et al. Local electronic structure of a single-layer porphyrin-containing covalent organic framework. *ACS Nano* **12**, 385–391 (2018).
23. Joshi, T. et al. Local electronic structure of molecular heterojunctions in a single-layer 2D covalent organic framework. *Adv. Mater.* **0**, 1805941 (2018).
24. Lindoy L. F. *The Chemistry of Macrocyclic Ligand Complexes* (Cambridge Univ. Press, 1989).
25. Stoddart, J. F. The chemistry of the mechanical bond. *Chem. Soc. Rev.* **38**, 1802–1820 (2009).
26. Rambo, B. M., Gong, H.-Y., Oh, M. & Sessler, J. L. The "Texas-Sized" Molecular Box: A versatile building block for the construction of anion-directed mechanically interlocked structures. *Acc. Chem. Res.* **45**, 1390–1401 (2012).
27. Stoddart, J. F. Mechanically interlocked molecules (MIMs)—molecular shuttles, switches, and machines (Nobel Lecture). *Angew. Chem., Int. Ed.* **56**, 11094–11125 (2017).
28. Li, Q. et al. Docking in metal–organic frameworks. *Science* **325**, 855 (2009).
29. Vukotic, V. N., Harris, K. J., Zhu, K., Schurko, R. W. & Loeb, S. J. Metal–organic frameworks with dynamic interlocked components. *Nat. Chem.* **4**, 456–460 (2012).
30. Li, X. et al. Rapid, scalable construction of highly crystalline acylhydrazone two-dimensional covalent organic frameworks via dipole-induced antiparallel stacking. *J. Am. Chem. Soc.* **142**, 4932–4943 (2020).
31. Allwood B. L., Spencer N., Shahriari-Zavareh H., Stoddart J. F. & Williams D. J. Complexation of Paraquat by a bisparaphenylene-34-crown-10 derivative. *J. Chem. Soc. Chem. Commun.* 1064–1066 (1987).
32. Li, X. et al. Tuneable near white-emissive two-dimensional covalent organic frameworks. *Nat. Commun.* **9**, 2335 (2018).
33. Anelli, P. L. et al. Molecular meccano. 1. [2]Rotaxanes and a [2]catenane made to order. *J. Am. Chem. Soc.* **114**, 193–218 (1992).
34. Poizat, O., Sourisseau, C. & Mathey, Y. Vibrational study of the methyl viologen dication MV^{2+} and radical cation $MV^{\cdot+}$ in several salts and as an intercalate in some layered MPS_3 compounds. *J. Chem. Soc. Faraday Trans.* **80**, 3257–3274 (1984).
35. Shearer, C. J., Slattery, A. D., Stapleton, A. J., Shapter, J. G. & Gibson, C. T. Accurate thickness measurement of graphene. *Nanotechnology* **27**, 125704 (2016).

Methods

Synthesis of MCOF-1. CyHz1 (23.1 mg, 0.03 mmol) and **Sa** (10.7 mg, 0.06 mmol) were mixed and sonicated with mesitylene (1 ml) in a Schlenk tube (10 ml, 15 mm × 80 mm) for 5 min. The mixture was added with 6 M acetic acid (aq, 0.1 ml) and sonicated for another 5 min, then flash frozen at 77 K, and degassed under freeze–pump–thaw for three cycles. The tube was sealed and heated at 120 °C for seven days. The solid obtained was exchanged with THF (5 ml) five times and dried under vacuum for 8 h to afford a yellow solid (26.1 mg, 93%). Anal. calcd. for $(C_{132}H_{144}N_{24}O_{46})_n$: C 56.57; H 5.18; N 11.99; found: C 57.62; H 5.04; N 10.06.

Synthesis of RCOF-1. CyHz1 (23.1 mg, 0.03 mmol), **Sa** (10.7 mg, 0.06 mmol) and **MVPF$_6$** (14.3 mg, 0.03 mmol) were mixed and sonicated with mesitylene (1 ml) in a Schlenk tube (10 ml, 15 mm × 80 mm) for 5 min. The mixture was added to 6 M acetic acid (aq, 0.1 ml) and sonicated for another 5 min, then flash frozen at 77 K, and degassed under freeze–pump–thaw for three cycles. The tube was sealed and heated at 120 °C for seven days. The solid obtained was exchanged with THF (5 ml × 1), water (5 ml × 2), and THF (5 ml × 2) and dried under vacuum for 8 h to afford a red solid (37.8 mg, 89%). Anal. calcd. for $(C_{168}H_{186}N_{30}O_{46}F_{36}P_6)_n$: C 47.69; H 4.43; N 9.93; found: C 48.48; H 4.86; N 8.85.

Synthesis of MCOF-0. CyHz0 (24.5 mg, 0.0375 mmol) and **Sa** (4.5 mg, 0.025 mmol) were mixed and sonicated with mesitylene (0.5 ml) in a Schlenk tube (10 ml, 15 mm × 80 mm) for 5 min. The mixture was added with 6 M acetic acid (aq, 50 µl) and sonicated for another 5 min, then flash frozen at 77 K, and degassed under freeze–pump–thaw for three cycles. The tube was sealed and heated at 120 °C for seven days. The solid obtained was exchanged with THF (5 ml) five times and dried under vacuum for 8 h to afford a yellow solid (24.3 mg, 88%). Anal. calcd. for $(C_{54}H_{66}N_6O_{19})_n$: C 58.79; H 6.03; N 7.62; found: C 56.72; H 5.88; N 7.44.

Synthesis of RCOF-0. CyHz0 (24.5 mg, 0.0375 mmol), **Sa** (4.5 mg, 0.025 mmol) and **MVPF$_6$** (17.8 mg, 0.0375 mmol) were mixed and sonicated with mesitylene (0.5 ml) in a Schlenk tube (10 ml, 15 mm × 80 mm) for 5 min. The mixture was added with 6 M acetic acid (aq, 50 µl) and sonicated for another 5 min, then flash frozen at 77 K, and degassed under freeze–pump–thaw for three cycles. The tube was sealed and heated at 120 °C for seven days. The solid obtained was exchanged with THF (5 ml × 1), water (5 ml × 2), and THF (5 ml × 2) and dried under vacuum for 8 h to afford a red solid (38.6 mg, 85%). Anal. calcd. for $(C_{72}H_{87}N_9O_{19}F_{18}P_3)_n$: C 47.58; H 4.83; N 6.94; found: C 42.25; H 5.01; N 6.96.

Data availability

X-ray crystallographic data have been deposited at the Cambridge Crystallographic Data Centre (http://www.ccdc.cam.ac.uk/) with CCDC reference numbers 1863696 (single-crystal **Cy1-MVPF$_6$**), and 2006788 (single-crystal **CyHz0-MVPF$_6$**). A copy of the data can be obtained free of charge via https://www.ccdc.cam.ac.uk/structures/. All other data supporting the findings of this study are available within the paper and its Supplementary Information. Data are also available from the corresponding author upon reasonable request.

Acknowledgements

K.P.L. acknowledges NRF-CRP grant "Two-Dimensional Covalent Organic Framework: Synthesis and Applications," grant number NRF-CRP16-2015-02, funded by National Research Foundation, Prime Minister's Office, Singapore. We acknowledge the use of the imaging facilities at the Center for BioImaging Sciences. Funding for the K2-IS camera is provided by the Singapore National Research Foundation's Competitive Research Program (NRF-CRP16-2015-05). We thank S. Xiangyan for the solid-state NMR measurement. We thank C. Hyun and T. J. Shin for the synchrotron-based GIXRD measurements.

Author contributions

Under the supervision of K.P.L., X.L. designed and performed most of the experiments, including synthesis and characterization of COFs and their model compounds. X.L., H.-S.X. and Q.G. discussed the manuscript. K.L. performed the AFM measurements. Under the supervision of U.M., S.W.C. performed and analysed the TEM of COFs, and N.J. performed and analysed SAED of COFs. X.Z. analysed the TEM results. H.X. performed the Q-plus AFM measurement. Under the supervision of S.Y.Q., J.Q. performed the DFT theoretical calculations. I.-H.P. resolved the single-crystal structures of the model compounds. X.L. and K.P.L. co-wrote the manuscript.

Competing interests

The authors declare no competing interests.

Additional information

Supplementary information is available for this paper at https://doi.org/10.1038/s41557-020-00562-5.

Correspondence and requests for materials should be addressed to K.P.L.

Reprints and permissions information is available at www.nature.com/reprints.